

Logarithmic Morphological Neural Nets robust to lighting variations^{*}

Guillaume Noyel¹[0000-0002-7374-548X], Emile
Barbier--Renard¹[0000-0003-2967-6082], Michel Jourlin¹[0000-0002-2076-3465], and
Thierry Fournel¹[0000-0002-1613-4594]

Laboratoire Hubert Curien, UMR CNRS 5516, Université Jean Monnet, 42 000
Saint-Etienne, France

{guillaume.noyel,michel.jourlin,fournel}@univ-st-etienne.fr
emile.barbier.renard@etu.univ-st-etienne.fr

Abstract. Morphological neural networks allow to learn the weights of a structuring function knowing the desired output image. However, those networks are not intrinsically robust to lighting variations in images with an optical cause, such as a change of light intensity. In this paper, we introduce a morphological neural network which possesses such a robustness to lighting variations. It is based on the recent framework of Logarithmic Mathematical Morphology (LMM), i.e. Mathematical Morphology defined with the Logarithmic Image Processing (LIP) model. This model has a LIP additive law which simulates in images a variation of the light intensity. We especially learn the structuring function of a LMM operator robust to those variations, namely : the map of LIP-additive Asplund distances. Results in images show that our neural network verifies the required property.

Keywords: Morphological neural nets · Logarithmic Image Processing · Logarithmic Mathematical Morphology · Robustness to lighting variations · Functional Asplund metric.

1 Introduction

Deep learning [8] based on convolutional neural networks (CNN) [16] has emerged as a methodology to learn a model of the data in order to perform a classification or a regression task [9]. During the training phase, the model parameters are learnt by minimising a loss between a given truth and the model prediction. In parallel to CNN, several morphological neural nets have been defined and studied. First, fully connected morphological neural nets (where the output depends on all the input pixels) have been defined in [6] and more recently by Charisopoulos et al. [5], Mondal et al. [21] and Zhang et al. [35]. Second, Barrera et al. defined morphological neural nets in sliding windows [2] (where the output only depends on the input pixels in the window). Moreover, deep morphological networks have also been defined by using either approximations of

^{*} Supported by Lyon Informatics Federation, France, through the “FakeNets” project.

the morphological operations [17,18,20,29,31,15,1], or exact morphological operations [7,23]. Deep morphological networks have been used e.g. for classification in hyperspectral images [23], image de-hazing or de-raining [19], image denoising [7]. A morphological network has a constant additive invariance [32]. In classical neural networks, a CNN was designed to have a shift invariance [4] and a neural net has a contrast invariance based on quaternion local phase [22].

However, morphological neural networks are not intrinsically robust to real lighting variations. The analysis of images presenting such variations is a challenging task that can occur in many settings [13,34,27]: industry, traffic control, underwater vision, face recognition, large public health databases, etc. In this paper, we propose a morphological neural network which is robust to such lighting variations due to a change of light intensity or of camera exposure-time.

Such a neural net is based on a metric, namely the functional Asplund metric [11] which presents this robustness property. This metric is defined with the *Logarithmic Image Processing* (LIP) model [12,13] which models those lighting variations. As the LIP model is based on a famous optical law, namely the *Transmittance Law*, we shall introduce in this way *Physics* in those neural nets. In addition, the maps of Asplund distances between an image and a reference template, the probe, are related to Mathematical Morphology [27]. We shall see that they are especially related to the newly introduced framework of *Logarithmic Mathematical Morphology* [24,25].

2 Background

2.1 Logarithmic Image Processing

The LIP model is defined for an image f acquired by transmission and, as it is consistent with the human vision [3,13], it can also be used for images acquired by reflection. In this model, the light is passing through a semi-transparent medium and is captured by the sensor. The resulting image f is a function defined on a domain $D \subset \mathbb{R}^2$ with values lying in the interval $[0, M[\subset \mathbb{R}$. It is important to note that the LIP greyscale is inverted with respect to the usual grey scale. 0 corresponds to the white extremity, when all the light passes through the medium. M is the black extremity, when no light is passing. For images digitised on 8-bits, M is always equal to $2^8 = 256$.

According to the *transmittance law*, the transmittance $T_{f \triangle g}$ of the superimposition $f \triangle g$ of two media which generate the images f and g , is equal to the product of the transmittances T_f and T_g of each image: $T_{f \triangle g} = T_f \cdot T_g$. The transmittance T_f of any medium generating the image f is equal to $T_f = 1 - f/M$. From both previous equations, the LIP-addition law is deduced :

$$f \triangle g = f + g - f \cdot g/M. \quad (1)$$

As the addition $f \triangle f$ may be written as $2 \triangle f$, the LIP-multiplication of an image f by a real number λ is expressed as:

$$\lambda \triangle f = M - M(1 - f/M)^\lambda. \quad (2)$$

When $\lambda = -1$, the LIP-negative function $\triangle f = -1 \triangle f$ can be defined, as well as the LIP-difference $f \triangle g$ between two images f and g . They are expressed as follows:

$$\triangle f = (-f)/(1 - f/M), \quad (3)$$

$$f \triangle g = (f - g)/(1 - g/M). \quad (4)$$

It can be noticed that $f \triangle g$ is an image (i.e. $f \triangle g \geq 0$) if and only if $f \geq g$.

The LIP model has a *strong mathematical property*. Let $\mathcal{F}_M =]-\infty, M[$ be the set of real functions defined on the domain D and whose values are less or equal than M . Let $\mathcal{I} = [0, M]^D$ be the set of images. The set $(\mathcal{F}_M, \triangle, \triangle)$ is a *real vector space* and the set $(\mathcal{I}, \triangle, \triangle)$ is its *positive cone*.

The LIP model also possesses a *strong physical property*. The LIP-negative values $\triangle f$, where $f \geq 0$, acts as light intensifiers. Those values can therefore be used to compensate the image attenuation in scenes captured with a low lighting. In particular, the LIP-addition of a positive constant to an image simulates the effect of a decrease of the light intensity or a decrease of the camera exposure-time. The resulting image is therefore darker than the original one. In an equivalent way, the LIP-subtraction of a positive constant from an image, simulates an increase and the resulting image becomes brighter.

2.2 Logarithmic Mathematical Morphology

Logarithmic Mathematical Morphology (LMM) was introduced by Noyel in [24,25]. LMM consists of defining morphological operations [30,10] in the LIP framework. In LMM, the dilation δ_b^\triangle and the erosion ϵ_b^\triangle are defined in the lattice (\mathcal{F}_M, \leq) . Let f and $b \in \overline{\mathcal{F}}_M$ be two functions, where $\overline{\mathcal{F}}_M = [-\infty, M]^D$. The function $b : D \mapsto]-\infty, M[$ is chosen as the structuring function, which implies that outside the domain $D_b \subset D$, all its values are equal to $-\infty$: $\forall x \in D \setminus D_b$, $b(x) = -\infty$. Both mappings δ_b^\triangle and ϵ_b^\triangle are named *logarithmic-dilation* and *logarithmic-erosion*, respectively. They are defined by:

$$\delta_b^\triangle(f)(x) = \vee \{f(x-h) \triangle b(h), h \in D\} \quad (5)$$

$$\epsilon_b^\triangle(f)(x) = \wedge \{f(x+h) \triangle b(h), h \in D\}. \quad (6)$$

In the case of ambiguous expressions, the following conventions will be used: $f(x-h) \triangle b(h) = -\infty$ when $f(x-h) = -\infty$ or $b(h) = -\infty$, and $f(x+h) \triangle b(h) = M$ when $f(x+h) = M$ or $b(h) = -\infty$.

Both operations form an adjunction, i.e. for all $f, g \in \mathcal{F}_M$, $\delta_b^\triangle(g) \leq f \Leftrightarrow g \leq \epsilon_b^\triangle(f)$. As a consequence, the composition $\gamma_b^\triangle = \delta_b^\triangle \circ \epsilon_b^\triangle$ is an *opening* and the composition $\varphi_b^\triangle = \epsilon_b^\triangle \circ \delta_b^\triangle$ is a *closing*. LMM operations are adaptive to lighting variations modelled by the LIP-additive law. We shall see that at least an operation which is robust to those lighting variations can be defined in the LMM framework.

The logarithmic-dilation δ_b^\triangle and the logarithmic-erosion ϵ_b^\triangle , which are defined in the lattice (\mathcal{F}_M, \leq) , are related to the usual functional dilation δ_b (or \oplus) and erosion ϵ_b (or \ominus), which are defined in the lattice of real functions (\mathbb{R}^D, \leq) .

These usual dilation and erosion are defined, for all $x \in D$, by :

$$\delta_b(f)(x) = (f \oplus b)(x) = \vee \{f(x-h) + b(h), h \in D\} \quad (7)$$

$$\varepsilon_b(f)(x) = (f \ominus b)(x) = \wedge \{f(x+h) - b(h), h \in D\}. \quad (8)$$

Such relations are based on the isomorphism $\xi : \overline{\mathcal{F}}_M \mapsto \overline{\mathbb{R}}^D$ and its inverse $\xi^{-1} : \overline{\mathbb{R}}^D \mapsto \overline{\mathcal{F}}_M$, which are expressed by $\xi(f) = -M \ln(1 - f/M)$ and $\xi^{-1}(f) = M(1 - \exp(-f/M))$ [14]. The relations between the logarithmic-operations δ_b^Δ , ε_b^Δ and the usual functional erosion are the following ones [24,25]:

$$\delta_b^\Delta(f) = \xi^{-1}(\delta_{\xi(b)}[\xi(f)]) = \xi^{-1}[\xi(f) \oplus \xi(b)] \quad (9)$$

$$\varepsilon_b^\Delta(f) = \xi^{-1}(\varepsilon_{\xi(b)}[\xi(f)]) = \xi^{-1}[\xi(f) \ominus \xi(b)], \quad (10)$$

where f and $b \in \mathbb{R}^D$. These relations are not only important from a theoretical point of view but also from a practical point of view. Indeed, they facilitate the programming of the logarithmic operations by using the usual morphological operations which exist in numerous image analysis software.

In Fig. 1, in an image f , the logarithmic-erosion $\varepsilon_b^\Delta(f)$ and dilation $\delta_b^\Delta(f)$ are compared to the usual erosion $\varepsilon_b(f)$ and dilation $\delta_b(f)$. For the logarithmic operations, the amplitude of the structuring function b varies according to the amplitude of the image f ; whereas, for the usual morphological operations, the amplitude of b does not change. In Fig. 1a, when the image intensity is close to the maximal possible value $M = 256$, the intensity of the logarithmic-dilation of f , $\delta_b^\Delta(f)$, is less or equal than M , because the structuring function becomes flat; whereas the intensity of the usual dilation of f , $\delta_b(f)$, is greater than M .

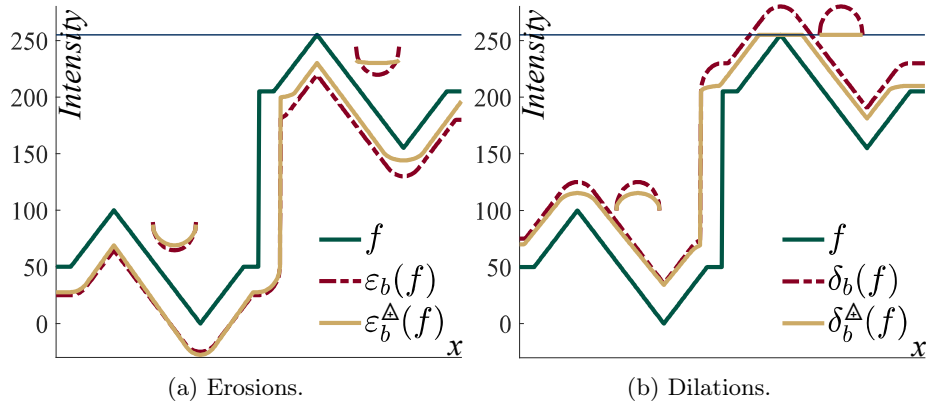


Fig. 1: In an image f , comparison between functional MM and LMM for the (a) erosions $\varepsilon_b(f)$, $\varepsilon_b^\Delta(f)$ and (b) dilations $\delta_b(f)$, $\delta_b^\Delta(f)$. (a) and (b) For both signal peaks, the structuring function b is represented (after an horizontal translation) for the erosions $\varepsilon_b(f)$, $\varepsilon_b^\Delta(f)$ and the dilations $\delta_b(f)$, $\delta_b^\Delta(f)$.

2.3 The LIP-additive Asplund metric

The LIP-additive Asplund metric was defined by Jourlin [11].

Definition 1 (LIP-additive Asplund metric). Let f and $g \in \mathcal{F}_M$ be two functions. One of them, e.g. g , is chosen as a probing function. Both following numbers are then defined by: $c_1 = \inf \{c, f \leq c \triangle g\}$ and $c_2 = \sup \{c, c \triangle g \leq f\}$, where c lies within the interval $]-\infty, M[$. The LIP-additive Asplund metric d_{asp}^\triangle is defined by

$$d_{asp}^\triangle(f, g) = c_1 \triangle c_2. \quad (11)$$

Property 1 (Robustness to lighting variations [11]). Importantly, this metric is invariant under lighting changes modelled by a LIP-addition of a constant:

$$\forall k \in]-\infty, M[, \quad d_{asp}^\triangle(f, g) = d_{asp}^\triangle(f \triangle k, g) \text{ and } d_{asp}^\triangle(f, f \triangle k) = 0. \quad (12)$$

Those changes correspond to a modification of the light intensity or of the camera exposure-time.

2.4 Learning of the structuring function in morphological operations

For machine learning in Mathematical Morphology (MM), the functions are defined in discrete grids of \mathbb{Z}^2 ; $f : D \mapsto \mathbb{R}$ and $b : D_b \mapsto \mathbb{R}$, where $D_b \subset D \subset \mathbb{Z}^2$. Let the cardinal of the set D_b be equal to $2n+1$. The bidimensional functions can always be represented as unidimensional arrays, e.g. by concatenating their rows. The structuring function are therefore written as follows: $b = \{b_{-n}, \dots, b_n\}$. The dilation δ_b and the erosion ε_b layers can be expressed by [7,19]:

$$\delta_b(f)(x) = \max_{i \in [-n, n]} \{f(x-i) + b_i\} \quad (13)$$

$$\varepsilon_b(f)(x) = \min_{i \in [-n, n]} \{f(x+i) - b_i\}. \quad (14)$$

An image f is passed through a dilation layer or an erosion layer that gives an output equal to \hat{g} (i.e. $\hat{g} = \delta_b(f)$ or $\hat{g} = \varepsilon_b(f)$). The weights of the structuring function b are learnt so that the loss $L(b) = L(g, \hat{g})$ between the output \hat{g} of the neural net layer and the desired output g , is minimised. The loss minimisation is performed by a *stochastic gradient descent* algorithm [8], which requires to compute the derivative of each weight to the loss:

$$\frac{\partial L}{\partial b_i} = \sum_x \frac{\partial \hat{g}(x)}{\partial b_i} \frac{\partial L}{\partial \hat{g}(x)} = \sum_x \nabla \hat{g}(x) \frac{\partial L}{\partial \hat{g}(x)}. \quad (15)$$

Let us denote $i^{x*} = \arg \max_{i \in [-n, n]} \{f(x-i) + b_i\}$ or $i^{x*} = \arg \min_{i \in [-n, n]} \{f(x+i) - b_i\}$, the index for which the dilation or the erosion takes its value. For the dilation, the gradient $\nabla \hat{g}$ is equal to :

$$\nabla \hat{g}(x) = \begin{cases} 1 & \text{if } \hat{g}(x) = f(x - i^{x*}) + b_{i^{x*}} \\ 0, & \text{otherwise} \end{cases} \quad (16)$$

and for the erosion to

$$\nabla \hat{g}(x) = \begin{cases} -1 & \text{if } \hat{g}(x) = f(x + i^{x*}) - b_{i^{x*}} \\ 0, & \text{otherwise.} \end{cases} \quad (17)$$

The structuring function is therefore updated as : $b(x) = b(x) - \alpha \partial L / \partial b(x)$.

3 Maps of LIP-additive Asplund distances

3.1 Definition

Definition 2 (Map of LIP-additive Asplund distances). Let $f \in \mathcal{F}_M$ be a function and $b \in]-\infty, M[^{D_b}$ a probe, where $D_b \subset D$. The map of Asplund distances is the mapping $Asp_b^\Delta : \mathcal{F}_M \mapsto \mathcal{I}$ defined by:

$$Asp_b^\Delta f(x) = d_{asp}^\Delta(f|_{D_b(x)}, b), \quad (18)$$

where $f|_{D_b(x)}$ is the restriction of f to the neighbourhood $D_b(x)$ centred on $x \in D$. The LIP addition Δ makes the map of distances robust to contrast variations due to exposure-time changes: $\forall c \in]-\infty, M[, Asp_b^\Delta(f \Delta c) = Asp_b^\Delta(f)$.

3.2 Link with Logarithmic Mathematical Morphology

The map of Asplund distances is related to Mathematical Morphology (MM) [26,27]. Noyel as shown in [25] that it is specifically related to LMM as follows.

Proposition 1. Let $f \in \overline{\mathcal{F}}_M$ be a function and $b \in \overline{\mathcal{F}}_M$ be a structuring function, where for all $x \in D_b$, $D_b \subset D$, $b(x) > -\infty$. The map of Asplund distances between the function f and the structuring function b is equal to:

$$Asp_b^\Delta f = \delta_{\Delta \bar{b}}^\Delta(f) \Delta \varepsilon_b^\Delta(f). \quad (19)$$

\bar{b} is the reflected structuring function defined by $\forall x \in \overline{D}_b$, $\bar{b}(x) = b(-x)$. In the case of ambiguous expressions, the following conventions will be used: $Asp_b^\Delta f(x) = M$ when $\delta_{\Delta \bar{b}}^\Delta(f)(x) = M$ or $\varepsilon_b^\Delta(f)(x) = -\infty$, and $Asp_b^\Delta f(x) = 0$ when $\delta_{\Delta \bar{b}}^\Delta(f)(x) = \varepsilon_b^\Delta(f)(x)$.

4 Neural net of map of Asplund distances

From equations (19), (9), (10) and knowing that $\xi(\Delta b) = -\xi(b)$ and $\xi(f \Delta g) = \xi(f) - \xi(g)$, one deduces that:

$$Asp_b^\Delta f = \xi^{-1} \left[\delta_{-\xi(\bar{b})} \xi(f) - \varepsilon_{\xi(b)} \xi(f) \right]. \quad (20)$$

We then create a *map of Asplund distance layer* Asp_b^Δ , where we apply this layer to the input image f in order to give an output $\hat{g} = Asp_b^\Delta(f)$. The structuring function b is learnt so as to minimise a loss $L(b) = L(g, \hat{g})$ between \hat{g} and a desired output $g = Asp_{b_r}^\Delta(f)$, where b_r is a reference structuring function. The goal is to learning b in order to discover b_r .

In morphological neuron implementations [7], learning b is equivalent to learn the weight matrix $W \in \mathbb{R}^{A \times B}$, where $W(x) = b(x)$, for all $x \in D_b$ and $W(x) = -\infty$, otherwise. $A \times B$ is the window size in pixels of $D_W \subset D$. However, in equation (19), in the term $\delta_{\Delta \bar{b}}^\Delta$, we also expect that for all $x \notin D_b$, $\Delta \bar{W}(x) = -\infty$, which is not compatible with the current definition of W .

We therefore introduce a definition of b relying on two learnt kernels: the height kernel W_h and the mask kernel $W_m \in \mathbb{R}^{A \times B}$. First, W_h corresponds to

the height-map of the probe satisfying $W_h(x) = b(x)$, for all $x \in D_b$. Second, W_m characterises the definition domain of the probe $D_b = \{x \in D_{W_m} \mid W_m(x) > 0\}$. We then rewrite equation (20) as:

$$Asp_b^{\Delta} f = \xi^{-1} [\delta_{b_{dil}}(\xi(f)) - \varepsilon_{b_{ero}}(\xi(f))], \quad (21)$$

where, $\forall x \in D_{W_m}$:

$$b_{dil}(x) = \begin{cases} -\xi(\overline{W_h})(x) & \text{if } \overline{W_m}(x) > 0 \\ -\infty & \text{otherwise} \end{cases}, b_{ero}(x) = \begin{cases} \xi(W_h)(x) & \text{if } W_m(x) > 0 \\ -\infty & \text{otherwise} \end{cases}. \quad (22)$$

In order to ensure that the gradient descent is smooth, a soft-binarisation function $\chi : \mathbb{R}^{A \times B} \mapsto]0, 1[^{A \times B}$, such as the sigmoid $\chi(v) = 1/(1 + \exp(-v))$, is applied to the mask kernel W_m instead of a threshold. We therefore define $V = \chi(W_m) \in]0, 1[^{A \times B}$ as the soft-mask of the probe in the window of size $A \times B$. Because V is not a binary mask, $-\infty$ cannot be used when computing b_{ero} or b_{dil} . As f is an image, we have for all $x \in D$, $f(x) \in [0, M - 1]$. This implies that $\xi(f(x)) \in [0, \xi(M - 1)]$. A bottom value $\perp = -\xi(M - 1)$ is chosen such that $\xi(f)(x) - \perp \geq \xi(M - 1)$. This implies that $\xi(f)(x) + \perp \geq \xi(0)$. We then define the approximations \tilde{b}_{dil} and \tilde{b}_{ero} of b_{dil} and b_{ero} as follows:

$$\tilde{b}_{dil} = -\xi(\overline{W_h}) \cdot \overline{V} + \perp \cdot (1 - \overline{V}) \quad (23)$$

$$\tilde{b}_{ero} = \xi(W_h) \cdot V + \perp \cdot (1 - \overline{V}). \quad (24)$$

From equations (21), (23), (24), an expression of \hat{g} is deduced:

$$\hat{g} = \xi^{-1} \left[\delta_{\tilde{b}_{dil}}(\xi(f)) - \varepsilon_{\tilde{b}_{ero}}(\xi(f)) \right]. \quad (25)$$

It only contains components with derivatives and which can be used in the back-propagation algorithm. In practice, W_h and W_m are both initialised as null matrices.

Remark 1. In order to push the weights of the kernel W_h away from zero, one might introduce a mean Gaussian or a mean squared Gaussian, as a regularisation function of W_m . This idea will be explored in future works.

5 Illustration and results

We have illustrated our LMM network by using the Fashion MNIST dataset composed of a training set of 60 000 images and a test set of 10 000 images [33]. Each image is digitised with a 8-bit greyscale and has a size of 28×28 pixels.

The goal was to learn a structuring function (or probe) b (represented by both matrices W_h and W_m) so as to discover a reference structuring function b_r . This reference structuring function was defined as follows, for all $x \in D_{W_{b_r}}$, where $D_{W_{b_r}} \subset D$ and W_{b_r} is a matrix of size 7×7 :

$$b_r(x) = \begin{cases} h(x) & \text{if } h(x) \geq 0, \text{ where } h(x) = -\beta\sqrt{7}\|x\|^2 \triangleq c \\ -\infty & \text{otherwise.} \end{cases} \quad (26)$$

Let $D_{b_r} = \{x \in D_{W_{b_r}} \mid h(x) \geq 0\}$ be the domain of the probe. The mask kernel $W_{m,r}$ and the height kernel $W_{h,r}$ of the reference structuring function b_r

are defined by $W_{m,r} = \mathbf{1}_{D_{b_r}}$ and $\forall x \in D_{W_{b_r}}, W_{h,r}(x) = b_r(x)$, if $x \in D_{b_r}$ and $W_{h,r}(x) = 0$, otherwise. $\mathbf{1}_{D_{b_r}}$ is the indicator function of the set D_{b_r} .

By varying the parameters $\beta \in \{0.2, 0.4, \dots, 1.2\}$ and $c \in \{10, 25, \dots, 250\}$, a total of 102 reference structuring functions b_r were generated. With those b_r , the desired outputs $g = \text{Asp}_{b_r}^{\Delta}(f)$ (i.e. a ground-truth) were computed in both train and test datasets. In the train set, the weights of b were learnt by minimising a loss $L(g, \hat{g})$. In the test set, the *map of Asplund distance layer* $\hat{g} = \text{Asp}_b^{\Delta}(f)$ was applied to the images f with the learnt structuring function b . The average of a validation metric Val_m was computed between the estimated outputs \hat{g} and the ground-truth g . For the loss L and the validation metric Val_m , we used the mean square error MSE or the LIP-mean square error $LIPMSE$ [28]:

$$MSE(g, \hat{g}) = \frac{1}{P} \sum_{i=1}^P [g_i - \hat{g}_i]^2 \quad (27)$$

$$LIPMSE(g, \hat{g}) = \frac{M^2}{P} \sum_{i=1}^P \left[\ln \left(\frac{M - g_i}{M - \hat{g}_i} \right) \right]^2, \quad (28)$$

where P is the number of pixels of g . The results of the validation metrics are shown in table 1. In order to verify the robustness to lighting variations of our neural network, we have performed two other experiments with the same train set, but two additional test sets. We had therefore three test sets. i) The first test set is the initial test set. ii) The second test set is composed of the images of the first test set which were darkened by LIP-adding to them a constant of 100. iii) The third test set is composed of the images of the first test set which were brightened by LIP-subtracting from them a constant of 100. In table 1, one can notice that the averaged validation metrics between the three test sets are similar with a residual difference less than 1.2×10^{-6} grey levels. Our neural network is therefore robust to lighting variations which are modelled by the LIP-addition of a constant.

Table 1: Comparison of the validations metrics Val_m in three test sets: average, standard deviation and absolute average differences with the ground truth of the 1st test set. Parameters: 15 epochs, Adam optimiser, learning rate $\alpha = 0.5$, batch size: 20.

Test sets	Metrics	Averages		Std dev.		Abs. av. diff.
1 st test set	MSE	9.740	$\times 10^{-5}$	0.673	$\times 10^{-3}$	
(initial, f)	$LIPMSE$	6.528	$\times 10^{-4}$	2.580	$\times 10^{-3}$	
2 nd test set	MSE	9.740	$\times 10^{-5}$	0.673	$\times 10^{-3}$	0
(dark, $f \triangle 100$)	$LIPMSE$	6.529	$\times 10^{-4}$	2.581	$\times 10^{-3}$	7×10^{-8}
3 rd test set	MSE	9.740	$\times 10^{-5}$	0.673	$\times 10^{-3}$	1×10^{-10}
(bright, $f \triangle 100$)	$LIPMSE$	6.516	$\times 10^{-4}$	2.576	$\times 10^{-3}$	1.2×10^{-6}

The error $E_{pr}(W_h, W_{h,r})$ between the height kernels of the learnt probe b and of the reference probe b_r is defined as follows:

$$E_{pr}(W_h, W_{h,r}) = \frac{1}{A.B} \left[\min_k \sum_{x \in D_{b_r}} (W_{h,r}(x) - (W_h(x) \triangle k))^2 + \sum_{x \notin D_{b_r}} W_h^2(x) \right] \quad (29)$$

It takes into account that the map of Asplund distances is invariant under the LIP-addition of a constant to its probe. Table 2 shows the average errors between the kernels W_m and W_h of the learnt structuring function b and the kernels $W_{m,r}$ and $W_{h,r}$ of the reference structuring function b_r , in the train set. One can notice that the average MSE between the soft mask kernels W_m and $W_{m,r}$ is very small, with a value in 1×10^{-5} . The average error between the height kernels W_h and $W_{h,r}$ has a value in 1×10^{-4} grey levels. This means that the learnt kernels W_m and W_h are similar to the reference kernels $W_{m,r}$ and $W_{h,r}$. The learnt probe b is therefore similar to the reference probe b_r .

Table 2: In the train set, comparison of the average errors between the kernels W_m and W_h of the learnt probe b and the kernels $W_{m,r}$, $W_{h,r}$ of the reference probe b_r . A total of 102 probes b have been learnt.

Kernels	Errors	Averages	Std dev.
Heights of the probe W_h	E_{pr}	6.89×10^{-5}	4.50×10^{-4}
Soft mask of the probe W_m	MSE	2.23×10^{-4}	7.74×10^{-4}

Figure 2 shows an image f of the test set (Fig. 2a). This image was darkened $f \triangle 100$ (Fig. 2b) or brightened $f \triangle 100$ (Fig. 2c). The ground-truth g was computed with the map of Asplund distances with the reference probe b_r : $g = Asp_{b_r}^{\triangle} f$ (Fig. 2d). The predictions \hat{g} of the maps of Asplund distances were made with the learnt structuring function b : (i) in the initial image: $Asp_b^{\triangle} f_1$ (Fig. 2e), (ii) in the darkened images: $Asp_b^{\triangle} (f_1 \triangle 100)$ (Fig. 2f) and (iii) in the brightened image: $Asp_b^{\triangle} (f_1 \triangle 100)$ (Fig. 2g). These images show that there is no noticeable differences between the predictions $Asp_b^{\triangle} f$, $Asp_b^{\triangle} (f \triangle 100)$, $Asp_b^{\triangle} (f \triangle 100)$ and the ground-truth $g = Asp_{b_r}^{\triangle} f$ and that the predictions are robust to lighting variations which are modelled by the LIP-addition or the LIP-subtraction of a constant. Figure 3 shows that the height kernels W_{h,b_r} of the reference probe b_r and W_h of the learnt probe b are similar. The mask kernels W_{m,b_r} and W_m are also similar.

6 Conclusion

We have introduced a logarithmic morphological neural network which is robust to real lighting variations. Those variations are modelled by the LIP-addition of a constant and they are caused by a change in the light intensity or in the camera exposure-time. Such a neural net is based on the functional Asplund metric defined with the LIP-additive law. In the future, by combining several

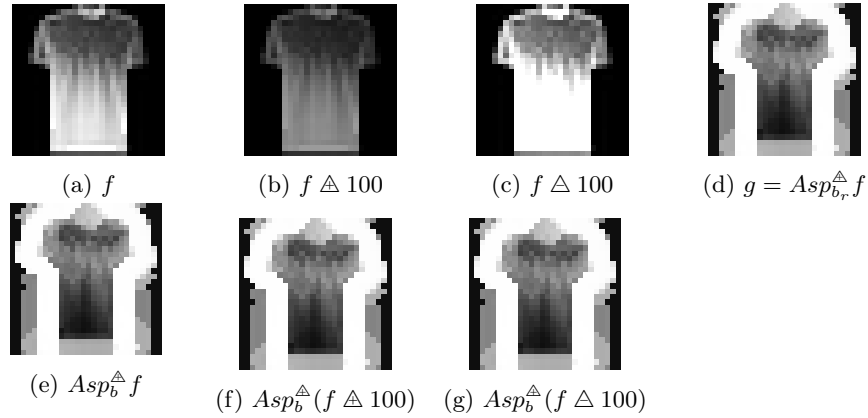


Fig. 2: (a) Image f coming from the Fashion MNIST test dataset. (b) $f \triangle 100$ darkened image. (c) $f \triangle 100$ brightened image. (d) $Asp_{b_r}^{\triangle} f$: ground-truth g , i.e. map of Asplund distances with the reference probe b_r . Predictions \hat{g} , i.e. maps of Asplund distances with the learnt probe b : (e) in the initial image $Asp_b^{\triangle} f$; (f) in the darkened image $Asp_b^{\triangle} (f \triangle 100)$; (g) in the brightened image $Asp_b^{\triangle} (f \triangle 100)$.

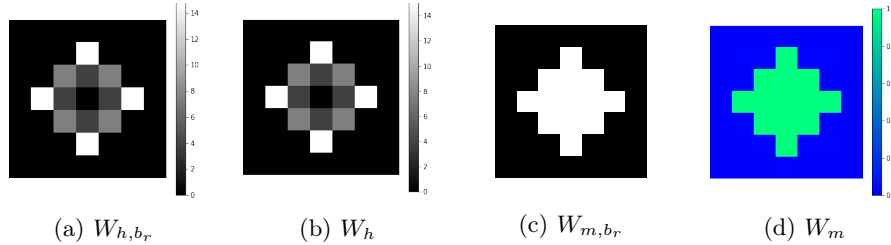


Fig. 3: In the inverted grey scale, height kernels (a) W_{h,b_r} of the reference probe b_r and (b) W_h of the learnt probe b . Mask kernels (c) W_{m,b_r} of the reference probe b_r and (d) W_m of the learnt probe b . As W_m is a soft mask, a color scale was used.

logarithmic morphological layers, we will define neural nets for numerous practical applications where the light is uncontrolled. We will also study neural nets for the LIP-multiplicative Asplund metric, which is invariant under changes of opacity. Such changes are modelled by the LIP-multiplication by a scalar.

References

1. Aouad, T., Talbot, H.: Binary morphological neural network (2022). <https://doi.org/10.48550/ARXIV.2203.12337>
2. Barrera, J., Dougherty, E.R., Tomita, N.S.: Automatic programming of binary morphological machines by design of statistically optimal operators in the context

- of computational learning theory. *Journal of Electronic Imaging* **6**(1), 54 – 67 (1997). <https://doi.org/10.1117/12.260010>
3. Brailean, J., Sullivan, B., Chen, C., Giger, M.: Evaluating the EM algorithm for image processing using a human visual fidelity criterion. In: ICASSP 1991. pp. 2957–2960 vol.4 (Apr 1991). <https://doi.org/10.1109/ICASSP.1991.151023>
 4. Chaman, A., Dokmanić, I.: Truly shift-invariant convolutional neural networks. In: CVPR 2021. pp. 3772–3782 (2021). <https://doi.org/10.1109/CVPR46437.2021.00377>
 5. Charisopoulos, V., Maragos, P.: Morphological perceptrons: Geometry and training algorithms. In: *Lect Notes Comput Sc.* vol. 10225, pp. 3–15. Springer, Cham (2017). https://doi.org/10.1007/978-3-319-57240-6_1
 6. Davidson, J.L., Hummer, F.: Morphology neural networks: An introduction with applications. *Circuits, Systems and Signal Processing* **12**(2), 177–210 (jun 1993). <https://doi.org/10.1007/BF01189873>
 7. Franchi, G., Fehri, A., Yao, A.: Deep morphological networks. *Pattern Recognition* **102**, 107246 (2020). <https://doi.org/10.1016/j.patcog.2020.107246>
 8. Goodfellow, I., Bengio, Y., Courville, A.: *Deep Learning*. MIT Press (2016), www.deeplearningbook.org
 9. Hastie, T., Tibshirani, R., Friedman, J.: *The Elements of Statistical Learning*. Springer, New York, NY, 2 edn. (2009). <https://doi.org/10.1007/978-0-387-84858-7>
 10. Heijmans, H., Ronse, C.: The algebraic basis of mathematical morphology I. Dilations and erosions. *Comput. Vision Graphics and Image Process.* **50**(3), 245 – 295 (Jun 1990). [https://doi.org/10.1016/0734-189X\(90\)90148-O](https://doi.org/10.1016/0734-189X(90)90148-O)
 11. Jourlin, M.: Chapter three - metrics based on logarithmic laws. In: *Logarithmic Image Processing: Theory and Applications*, *Adv. Imag. Electron Phys.*, vol. 195, pp. 61 – 113. Elsevier (2016). <https://doi.org/10.1016/bs.aiep.2016.04.003>
 12. Jourlin, M., Pinoli, J.: Logarithmic image processing: The mathematical and physical framework for the representation and processing of transmitted images. *Adv. Imag. Electron Phys.*, vol. 115, pp. 129 – 196. Elsevier (2001). [https://doi.org/10.1016/S1076-5670\(01\)80095-1](https://doi.org/10.1016/S1076-5670(01)80095-1)
 13. Jourlin, M.: *Logarithmic Image Processing: Theory and Applications*, *Adv. Imag. Electron Phys.*, vol. 195. Elsevier (2016)
 14. Jourlin, M., Pinoli, J.C.: Image dynamic range enhancement and stabilization in the context of the logarithmic image processing model. *Signal Process.* **41**(2), 225–237 (Jan 1995). [https://doi.org/10.1016/0165-1684\(94\)00102-6](https://doi.org/10.1016/0165-1684(94)00102-6)
 15. Kirszenberg, A., Tochon, G., Puybureau, É., Angulo, J.: Going beyond p-convolutions to learn grayscale morphological operators. In: *Lect Notes Comput Sc.* vol. 12708, pp. 470–482. Springer, Cham (2021). https://doi.org/10.1007/978-3-030-76657-3_34
 16. LeCun, Y., Bengio, Y., Hinton, G.: Deep learning. *Nature* **521**(7553), 436–444 (May 2015). <https://doi.org/10.1038/nature14539>
 17. Masci, J., Angulo, J., Schmidhuber, J.: A learning framework for morphological operators using counter-harmonic mean. In: *Lect Notes Comput Sc.* vol. 7883, pp. 329–340. Springer, Berlin, Heidelberg (2013). https://doi.org/10.1007/978-3-642-38294-9_28
 18. Mellouli, D., Hamdani, T.M., Ayed, M.B., Alimi, A.M.: Morph-CNN: A morphological convolutional neural network for image classification. In: *Lect Notes Comput Sc.* vol. 10635, pp. 110–117. Springer, Cham (2017). https://doi.org/10.1007/978-3-319-70096-0_12

19. Mondal, R., Dey, M.S., Chanda, B.: Image restoration by learning morphological opening-closing network. *Mathematical Morphology - Theory and Applications* **4**(1), 87–107 (2020). <https://doi.org/doi:10.1515/mathm-2020-0103>
20. Mondal, R., Mukherjee, S.S., Santra, S., Chanda, B.: Morphological Network: How Far Can We Go with Morphological Neurons? (jan 2019). <https://doi.org/10.48550/arxiv.1901.00109>
21. Mondal, R., Santra, S., Chanda, B.: Dense morphological network: An universal function approximator. *CoRR* (2019), <http://arxiv.org/abs/1901.00109>
22. Moya-Sánchez, E.U., Xambó-Descamps, S., Sánchez Pérez, A., Salazar-Colores, S., et al.: A bio-inspired quaternion local phase CNN layer with contrast invariance and linear sensitivity to rotation angles. *Pattern Recognition Letters* **131**, 56–62 (2020). <https://doi.org/10.1016/j.patrec.2019.12.001>
23. Nogueira, K., Chanussot, J., Mura, M.D., Santos, J.A.D.: An introduction to deep morphological networks. *IEEE Access* **9**, 114308–114324 (2021). <https://doi.org/10.1109/ACCESS.2021.3104405>
24. Noyel, G.: Logarithmic mathematical morphology: A new framework adaptive to illumination changes. *Lect Notes Comput Sc*, vol. 11401, pp. 453–461. Springer (2019). https://doi.org/10.1007/978-3-030-13469-3_53
25. Noyel, G.: Morphological and logarithmic analysis of large image databases. Dissertation of accreditation to supervise research, Université de Reims Champagne-Ardenne, France (Jun 2021), <https://tel.archives-ouvertes.fr/tel-03343079>
26. Noyel, G., Jourlin, M.: Double-sided probing by map of Asplund’s distances using logarithmic image processing in the framework of mathematical morphology. *Lect Notes Comput Sc*, vol. 10225, pp. 408–420. Springer (2017). https://doi.org/10.1007/978-3-319-57240-6_33
27. Noyel, G., Jourlin, M.: Functional asplund metrics for pattern matching, robust to variable lighting conditions. *Image Anal. Stereol.* **39**(2), 53–71 (2020). <https://doi.org/10.5566/ias.2292>
28. Pinoli, J.C.: Metrics, scalar product and correlation adapted to logarithmic images. *Acta Stereologica* **11**(2), 157–168 (1992), <https://popups.uliege.be:443/0351-580x/index.php?id=1901>
29. Saedan, F., Weber, N., Goesele, M., Roth, S.: Detail-preserving pooling in deep networks. In: *CVPR 2018*. pp. 9108–9116 (2018). <https://doi.org/10.1109/CVPR.2018.00949>
30. Serra, J.: *Image Analysis and Mathematical Morphology*, vol. 1. Academic, Orlando, FL, USA (1982)
31. Shen, Y., Zhong, X., Shih, F.Y.: Deep morphological neural networks. *CoRR* (2019), <http://arxiv.org/abs/1909.01532>
32. Velasco-Forero, S., Pagès, R., Angulo, J.: Learnable empirical mode decomposition based on mathematical morphology. *SIAM J. Imaging Sci.* **15**(1), 23–44 (2022). <https://doi.org/10.1137/21M1417867>
33. Zalando: Fashion MNIST. www.kaggle.com/datasets/zalando-research/fashionmnist (2017)
34. Zhang, W., Zhao, X., Morvan, J.M., Chen, L.: Improving shadow suppression for illumination robust face recognition. *IEEE T Pattern Anal* **41**(3), 611–624 (2019). <https://doi.org/10.1109/TPAMI.2018.2803179>
35. Zhang, Y., Blusseau, S., Velasco-Forero, S., Bloch, I., Angulo, J.: Max-plus operators applied to filter selection and model pruning in neural networks. In: *Lect Notes Comput Sc*. vol. 11564, pp. 310–322. Springer, Cham (2019). https://doi.org/10.1007/978-3-030-20867-7_24